ACS Photonics

Article

Cite This: ACS Photonics 2019, 6, 492−500

pubs.acs.org/journal/apchd5

Genuine Dynamics vs Cross Phase Modulation Artifacts in Femtosecond Stimulated Raman Spectroscopy

Giovanni Batignani,[†] Giuseppe Fumero,[†,‡] Emanuele Pontecorvo,[†] Carino Ferrante,[†,¶] Shaul Mukamel,[§] and Tullio Scopigno*[,†,¶]

[†]Dipartimento di Fisica, Universitá di Roma "La Sapienza", Roma, I-00185, Italy

[‡]Dipartimento di Scienze di Base e Applicate per l'Ingegneria, Universitá di Roma "La Sapienza", Roma, I-00161, Italy

[¶]Istituto Italiano di Tecnologia, Center for Life Nano Science @Sapienza, Roma, I-00161, Italy

[§]Department of Chemistry, University of California, Irvine, California 92697-2025, United States

Supporting Information

ABSTRACT: Femtosecond stimulated Raman scattering is a time-resolved vibrational spectroscopic technique able to access sub-picosecond dynamics and providing accurate structural information. Thanks to an appropriate combination of three laser pulses, triggering vibrational coherences delayed with respect to the photoinduced event of interest, it is capable of uncompromised temporal precision (down to 50 fs) and spectral resolution (a few wavenumbers), better than spontaneous Raman. Reaching such extreme time scales requires significant temporal overlap of pulses, which gives rise to undesired nonlinear artifacts, often hampering an immediate interpretation of the Raman spectra. Building on a perturbative expansion of the density matrix, we identify the origin of such artifacts in cross phase modulation effects and show how they can be theoretically evaluated and factored out from the signals. We experimentally benchmark the theoretical predictions in a nonreactive model system, namely cyclohexane.

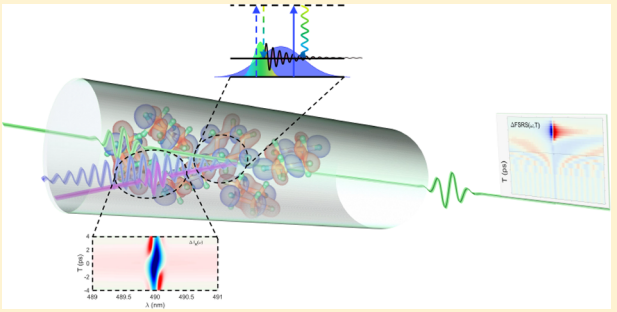

KEYWORDS: *nonlinear photonics, ultrafast spectroscopy, coherent Raman, cross phase modulation*

Ultrafast spectroscopy aims to investigate out-of-equilibrium phenomena in condensed matter and molecular systems, involving picosecond and sub-picosecond atomic structural rearrangement and electronic dynamics.[1] The standard time-resolved technique is the pump−probe scheme, where an actinic pump (AP) pulse photoexcites the system under investigation and a time-delayed probe monitors its subsequent dynamics, mapping the evolution from reactants to photoproducts. Among various pump−probe approaches, time-resolved spontaneous Raman (SPR) spectroscopy provides vibrational sensitivity, enabling access to structural and dynamical properties of the transient investigated species.[2−4] Critically, in SPR spectroscopy the temporal and energy resolutions are fundamentally constrained by the Fourier transform uncertainty, hampering the study of sub-picosecond phenomena. Femtosecond stimulated Raman scattering (FSRS)[5] offers the intriguing possibility of circumventing the time-resolved SPR limitations.[6] The technique combines a narrowband picosecond beam, referred as Raman pulse (RP), with a broadband femtosecond probe pulse (PP), monitoring the sample through a stimulated Raman scattering (SRS) process. Using an ultrashort broadband PP allows for coherent stimulation of molecular vibrations, which can be achieved for all the Raman active modes whose frequency corresponds to the energy difference between the RP and PP photons. Notably, the narrowband RP ensures high spectral resolution, over a wide accessible spectral region guaranteed by broadband PP pulse. Since the SRS process requires both fields to temporally overlap in the sample, the stimulation of vibrational coherences is triggered with a temporal precision determined by the shortest, femtosecond, PP. Moreover, the Raman spectra are engraved on top of the directional PP, ensuring an efficient isolation of the signal from the isotropic incoherent fluorescence background. The addition of a femtosecond actinic pump pulse, triggering a photoreaction, to the SRS detection scheme makes it possible to study structural changes in ultrafast photophysical and photochemical processes, providing both femtosecond temporal precision and atomic spectral resolutions.

During the past decade, the FSRS capabilities to unveil femtosecond structural changes have been road tested for a large scenario of samples, spanning from biochemical compounds to condensed-matter systems. Particularly, FSRS provided huge insights on the study of photoreaction processes,[7−10] on different protein structural evolution upon

Received: October 22, 2018
Published: January 14, 2019

DOI: 10.1021/acsphotonics.8b01467
ACS Photonics 2019, 6, 492−500

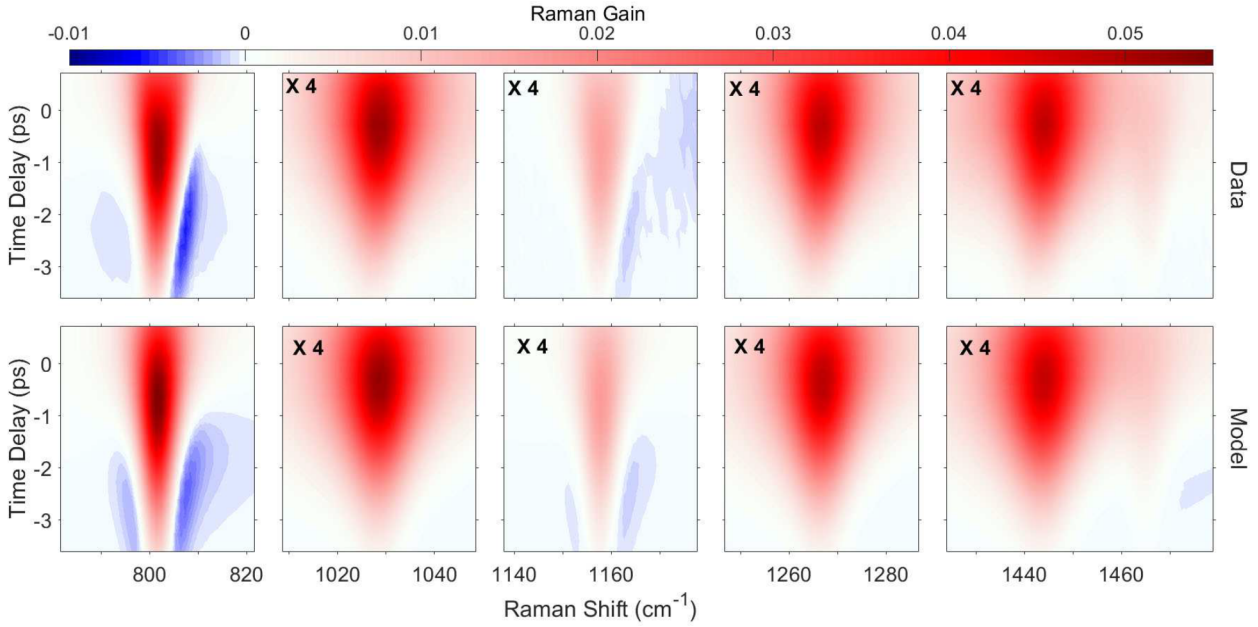

Figure 1. Broadband stimulated Raman spectra of liquid cyclohexane: Experimental (top panel) and simulated (bottom panel) nonresonant SRS spectrum measured without AP photoexcitation, as a function of Raman shift and relative delay between Raman and probe pulses. Six vibrational modes (at 801, 1028, 1158, 1266, 1444, 1465 cm^{-1}) are monitored in order to calibrate the experimental parameters for the FSRS experiment. Beyond 900 cm^{-1} the color maps have been 4× magnified. The relative amplitudes of the modes under consideration are 5.47, 3.28, 0.43, 2.91, 3.25, 0.19, while the line widths are 3.1, 13.4, 3.3, 12.7, 14.8, 7.0 (cm^{-1}). Small negative side wings, measured when the femtosecond probe pulse anticipates in time the RP maximum, occur for long-living vibrational coherences (801 and 1158 cm^{-1} modes), in agreement with the literature.[39,40]

photoexcitation,[11−13] on vibrational energy redistribution,[14,15] and on the wavepacket evolution on excited state surfaces.[16−22] In addition, FSRS has also been applied to investigate condensed matter compounds, with potential huge outcomes in the field of photonics, for measuring lattice dynamics in semiconductor nanocrystals,[23] for directly monitoring the ultrafast long-range charge separation,[24] and for unraveling photoinduced modification of magnetic properties.[25,26]

Understanding the joint spectral and temporal resolution limits of FSRS has drawn extensive experimental and theoretical attention.[27−29] For physical processes occurring on 100 fs (or faster) time scales, indeed, the dynamics of interest takes place in the temporal region in which all three pulses used in FSRS temporally overlap. Under this circumstance, the evolution monitored during the delay between the actinic and probe pulses contains the desired information as well as instrumental nonlinear contributions independent of the system dynamics, which are usually referred to as coherent artifacts,[30−34] hampering the detection and the interpretation of genuine FSRS signals.[26] In this work, we assign these features to a cross phase modulation (XPM)[35−38] effect, which originates from a pure optical coupling between the RP and the AP, and show how to model and subtract it from the experimental data.

RESULTS AND DISCUSSION

In Figure 1 we report the SRS measurement (without actinic photoexcitation) performed on a common solvent, liquid cyclohexane, as a function of the temporal delay ΔT_{R-P} between the Raman and the probe pulses. We used these measurements to calibrate the pulse parameters in the FSRS experiment. We focus on the red side of the spectrum (conventionally referred to as the Stokes side in spontaneous Raman spectroscopy), measured in the region at longer wavelength with respect to the RP. The reported stimulated Raman gain (SRG) is obtained as $\mathrm{SRG}(\omega) = \left(\frac{|E_P(\omega)|^2}{|E_P^0(\omega)|^2} - 1\right)$, where $|E_P(\omega)|^2$ and $|E_P^0(\omega)|^2$ indicate the PP spectrum measured with and without the presence of the RP. To avoid transient absorption modulation of the PP or promotion of the system to excited electronic states, both the RP and PP are tuned in the off-resonant condition, with an RP at 490 nm and a PP covering the 450−750 nm spectral range. Notably, the third-order nonlinear polarization $P^{(3)}$, which generates the SRS signal, can in principle originate from concurring processes, resulting from the different permutations of the fields interacting with matter.[41−43] However, in the off-resonant regime, the measured SRS signal is generated by a single dominant four-wave mixing contribution, which is depicted in Figure 2.

The third-order polarization $P^{(3)}$ induced in the sample can be calculated as[43−45]

$$P^{(3)}(t) = \left(-\frac{i}{\hbar}\right)^3 |\mu_{ab}|^2 |\mu_{bc}|^2 \int_0^\infty d\tau_3 \int_0^\infty d\tau_2 \int_0^\infty d\tau_1 \times \mathcal{E}_R^*(t-\tau_1-\tau_2-\tau_3)\mathcal{E}_P(t-\tau_2-\tau_3)\mathcal{E}_R(t-\tau_3) \times e^{i\omega_R(t-\tau_1-\tau_2-\tau_3)} e^{-i\omega_P(t-\tau_2-\tau_3)} e^{-i\omega_R(t-\tau_3)} e^{-i\tilde{\omega}_{ab}\tau_1} \times e^{-i\tilde{\omega}_{ac}\tau_2} e^{-i\tilde{\omega}_{bc}\tau_3} \quad (1)$$

where $\tilde{\omega}_{ij} = \omega_{ij} - i\gamma_{ij}$, $\omega_{ij} = \omega_i - \omega_j$ is the energy difference between the i and j levels, and $\gamma_{ij} = \tau_{ij}^{-1}$ is the dephasing rate of the $|i\rangle\langle j|$ coherence. $\mathcal{E}_R(t)$ and $\mathcal{E}_P(t)$ denote the temporal envelopes of the RP and PP fields, respectively, where $E_{R/P}^0(t) = \mathcal{E}_{R/P}(t)e^{-i\omega_{R/P}t} + \mathrm{c.c.}$ Labels a, c, and b indicate the ground state, the vibrational excited state, and the electronic excited state. The frequency dispersed signal can be obtained by Fourier transforming the nonlinear polar-

DOI: 10.1021/acsphotonics.8b01467
ACS Photonics 2019, 6, 492−500

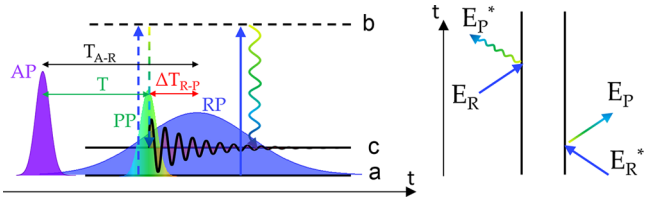

Figure 2. Pulse configuration and third-order diagram accounting for the measured SRS spectra: the energy level and double -sided Feynman diagrams representing the SRS process are depicted in the left and right panels, respectively. Two consecutive interactions between the molecule and the RP and PP fields stimulate a vibrational coherence, which is detected through a second interaction with the RP and a free induction decay, taking place within the vibrational coherence time and duration of the RP. Importantly, the FSRS signal is emitted along the PP direction, and it is self-phase-matched ($k_{FSRS} = -k_R + k_P + k_R = k_P$).[27,45] Dashed and continuous arrows indicate interactions with the bra and ket sides of the density matrix, respectively.

ization: $P^{(3)}(\omega) = \int_{-\infty}^{\infty} P^{(3)}(t) e^{i\omega t}\, dt$. To reduce the computational efforts required for calculating eq 1, it is useful to write all the pulse fields in the frequency domain

$$P^{(3)}(\omega) = \left(-\frac{i}{\hbar}\right)^3 |\mu_{ab}|^2 |\mu_{bc}|^2 \int_{-\infty}^{\infty} dt\, e^{i\omega t} \int_0^{\infty} d\tau_3 \int_0^{\infty} d\tau_2 \int_0^{\infty} d\tau_1 \times \int_{-\infty}^{\infty} d\omega_1 \int_{-\infty}^{\infty} d\omega_2 \int_{-\infty}^{\infty} d\omega_3 \times \mathcal{E}_R^*(\omega_1) e^{i(\omega_R+\omega_1)(t-\tau_1-\tau_2-\tau_3)} \mathcal{E}_P(\omega_2) e^{-i(\omega_P+\omega_2)(t-\tau_2-\tau_3)} \times \mathcal{E}_R(\omega_3) e^{-i(\omega_R+\omega_3)(t-\tau_3)} e^{-i\tilde{\omega}_{ab}\tau_1} e^{-i\tilde{\omega}_{ac}\tau_2} e^{-i\tilde{\omega}_{bc}\tau_3} \quad (2)$$

In this way, all the temporal integrals can be solved analytically, leading to

$$P^{(3)}(\omega) = |\mu_{ab}|^2 |\mu_{bc}|^2 \frac{1}{\tilde{\omega}_{bc} - \omega} \int_{-\infty}^{\infty} d\omega_1 \frac{\mathcal{E}_R^*(\omega_1)}{\omega_R + \omega_1 + \tilde{\omega}_{ab}} \times \int_{-\infty}^{\infty} d\omega_3 \frac{\mathcal{E}_R(\omega_3)\mathcal{E}_P(\omega - \omega_P + \omega_1 - \omega_3)}{\omega - \omega_3 - \omega_R - \tilde{\omega}_{ac}} \quad (3)$$

where the conservation of energy $\int_{-\infty}^{\infty} e^{i(\omega-\omega_P+\omega_1-\omega_3-\omega_2)t}\, dt = \delta(\omega - \omega_P + \omega_1 - \omega_3 - \omega_2)$ has been used to simplify the integral over $\omega_2 \in (-\infty, \infty)$.

When the RP temporal and spectral profiles do not vary across the sample, the SRS response can be calculated as

$$SRG(\omega) \propto \Im\left[\frac{P^{(3)}(\omega)}{E_P^0(\omega)}\right] \quad (4)$$

where $\Im$ denotes the imaginary part.

Equation 4 has been used to fit SRS spectra, and the results are reported in the bottom panel of Figure 1, where both the RP and the PP have been modeled with transform-limited Gaussian profiles, showing a fair agreement between experimental and fitted spectra for the delays spanning the whole RP temporal envelope.

In order to study the presence of nonlinear artifacts induced by the AP, resulting in spectral features not related to the system dynamics, we measured the FSRS spectra focusing on the sample a nonresonant pump (650 nm central wavelength), which mimics the electric field effect of the pump pulse required for monitoring transient dynamics in photochemically active systems. Under such conditions, no transient dynamics takes place, and hence the differences in the measured signal with respect to the SRG shown in Figure 1 can be ascribed to XPM between the AP and the RP. In order to isolate such nonlinear contributions, in Figure 3 we report the differential Raman gain, defined as $\Delta RG(\omega, T) = FSRG(\omega, T) - SRG(\omega)$, where $FSRG(\omega, T)$ and $SRG(\omega)$ indicate the Raman gain measured in the presence and absence of the AP, respectively. T is the time delay of the PP with respect to the

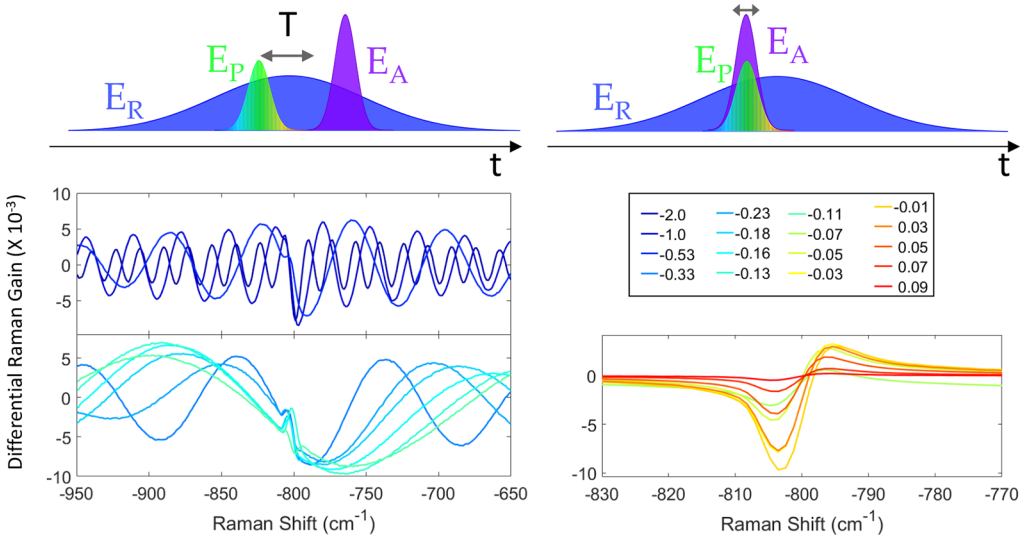

Figure 3. Experimental nonresonant FSRS spectra of cyclohexane: Differential Raman gain spectra $\Delta RG(\omega, T)$ around the 801 cm^{-1} Raman mode. For negative time delays T (i.e., for an AP following the PP), reported in the left panel, an oscillating signal extending to a spectral region much broader than the vibrational line width (~10 cm^{-1}) is measured. Notably, the frequency of the oscillations is directly proportional to the temporal delay between AP and PP. Within the overlap condition between AP and PP, reported in the right panel, an asymmetric dispersive feature centered around the peak position is observed. No features have been observed for positive time delays T, as expected in the absence of photoinduced dynamics. The values of the delays T in ps are reported in the legend. A sketch of the experimental pulse configurations is reported in the top panels.

DOI: 10.1021/acsphotonics.8b01467
ACS Photonics 2019, 6, 492−500

AP. Notably, any change in the measured signal due to XPM artifacts between the AP and the PP is ruled out since, as detailed in the Methods section, FSRG(ω, T) is computed with the $|E_P^0(\omega)|^2$ field measured in the presence of the AP.

As expected, for positive time delays, i.e., for an AP preceding the PP, when the AP−PP femtosecond pulses do not temporally overlap, the detected FSRG(ω, T) and SRG(ω) show no differences for any values of T and ΔRG(ω, T) vanishes. In contrast, within the AP−PP time-overlap region, the differential Raman gain shows a dispersive profile around the Raman line maximum. Under such conditions, the identification of peak position and spectral width is obscured, preventing the vibrational characterization of the sample. Notably, as shown in the left panel of Figure 3, the differential signal does not vanish even outside of the overlap condition, for negative time delays T, where we observe baseline oscillations, centered around the peak position and extending to a spectral region much broader than the vibrational line width. The frequency of this spectral modulation is inversely proportional to T, with a period $\Delta\omega_{osc}(\mathrm{cm}^{-1}) = \frac{100}{3T(\mathrm{ps})}$. These oscillating features cannot be ascribed to an AP photoinduced truncation of the vibrational coherence. In fact, such a hypothesis has to be ruled out on the basis of two points: (i) the nonresonant AP cannot promote the system to an excited electronic state, breaking the vibrational coherence; (ii) in contrast to the experimental data, showing a ΔRG(ω, T) decreasing for long time delays, a truncation of the vibrational coherence would result in a sinc-shaped FSRG(ω) signal, with a broadening and a drop of the peak amplitude at small T. Interestingly, similar oscillations have also been observed in the optical heterodyne detected birefringence response of electronically nonresonant liquids.[46]

In order to numerically calculate how XPM effects can modify FSRS spectra, we considered the evolution of the temporal and spectral properties of the pulses while crossing the sample. An electric field, propagating along the z direction, can be represented as

$$E_i(z, t) = A_i(z, t)e^{i(k_i z - \omega_i t)}$$

where the subscript i = P, R, A indicates the PP, the RP, and the AP and $A_i(z, t)$ is the envelope of the electric fields $E_i(z, t)$. For $A_i(z, t)$ satisfying the slowly varying envelope approximation, the wave equation describing the pulse propagation in linear, dispersive media, including linear ($\beta_1^{(i)} = \frac{\mathrm{d}k}{\mathrm{d}\omega}\Big|_{\omega=\omega_i} = v_g^{-1}$) and quadratic ($\beta_2^{(i)} = \frac{\mathrm{d}^2k}{\mathrm{d}\omega^2}\Big|_{\omega=\omega_i}$) dispersion effects, can be expressed as[36]

$$\frac{\partial A_i}{\partial z} + \beta_1^{(i)}\frac{\partial A_i}{\partial t} + \frac{i}{2}\beta_2^{(i)}\frac{\partial^2 A_i}{\partial t^2} = 0$$

which can be recast in the spectral domain as

$$\frac{\partial \tilde{A}_i}{\partial z} - i\beta_1^{(i)}\omega\tilde{A}_i - \frac{i}{2}\beta_2^{(i)}\omega^2\tilde{A}_i = 0 \quad (5)$$

Cross phase modulation arises when intense ultrashort pulses propagate together through a nonlinear medium and distort the electronic configuration of the material, modifying the refractive index. This, in turn, temporally and spatially modulates the fields phase, resulting in a transformation of the spectral properties of the pulses,[36−38] without inducing any energy transfer between them.

Notably, when the pulses are tuned in resonance with an electronic transition of the system under investigation, intensity and spectral profile modifications of the pulses across the sample can be taken into account including the absorption coefficient $\alpha(\omega)$ in eq 5:

$$\frac{\partial \tilde{A}_i}{\partial z} - i\beta_1^{(i)}\omega\tilde{A}_i - \frac{i}{2}\beta_2^{(i)}\omega^2\tilde{A}_i + \frac{\alpha(\omega)}{2}\tilde{A}_i = 0 \quad (6)$$

Since in this work we consider nonresonant beams, in the following equations we set $\alpha(\omega) = 0$.

XPM can affect FSRS signals when the picosecond RP field, at a frequency different with respect to the AP, propagates through a sample, whose refractive index is modified by the intense AP pulse.[43] The RP phase, and hence its spectral profile, is modulated by the temporal variation of the index of refraction originating from the presence of the intense AP. Under such conditions, the effect of XPM between two laser fields $E_i(z, t)$ and $E_j(z, t)$ can be described by the coupled nonlinear Schrödinger equations

$$\begin{aligned}\frac{\partial A_i}{\partial z} + \beta_1^{(i)}\frac{\partial A_i}{\partial t} + \frac{i}{2}\beta_2^{(i)}\frac{\partial^2 A_i}{\partial t^2} &= i\gamma(|A_i|^2 + 2|A_j|^2)A_i \\ \frac{\partial A_j}{\partial z} + \beta_1^{(i)}\frac{\partial A_j}{\partial t} + \frac{i}{2}\beta_2^{(i)}\frac{\partial^2 A_j}{\partial t^2} &= i\gamma(|A_j|^2 + 2|A_i|^2)A_j\end{aligned} \quad (7)$$

where γ takes into account the coupling between optical fields propagating in a nonlinear medium through cross-phase modulation, due to which each pulse experiences an effective refractive index that depends on the intensity of the other copropagating beams.[36,47] Working in a reference frame moving at the E_i field group velocity, eq 7 can be recast as

$$\begin{aligned}\frac{\partial A_i}{\partial z} + \frac{i}{2}\beta_2^{(i)}\frac{\partial^2 A_i}{\partial \tau^2} &= i\gamma(|A_i|^2 + 2|A_j|^2)A_i \\ \frac{\partial A_j}{\partial z} + \epsilon\frac{\partial A_j}{\partial \tau} + \frac{i}{2}\beta_2^{(i)}\frac{\partial^2 A_j}{\partial \tau^2} &= i\gamma(|A_j|^2 + 2|A_i|^2)A_j\end{aligned} \quad (8)$$

where $\epsilon = \beta_1^{(i)} - \beta_1^{(j)}$ and $\tau = t - \beta_1^{(i)}z$.

The pulse propagation can be calculated from eq 8 through a symmetrized split-step Fourier method: numerical integrations are performed at small steps of dz, separately evolving the linear and the nonlinear terms. The linear propagation of the A amplitudes is computed in the frequency domain accordingly to eq 5 for $dz/2$; then the nonlinear evolution is performed separately in the time domain for dz and the linear propagator is applied again for $dz/2$.

Notably, when the temporal and spectral properties of the RP used in an FSRS experiment vary across the sample (due to the dispersive and nonlinear terms appearing in eq 8), eq 4 is no longer valid to calculate the Raman gain. In fact, since molecules in distinct points of the sample interact with a different electromagnetic RP field, the nonlinear polarization induced in the sample depends on the position in which the interaction happens in the sample: $P^{(3)} = P^{(3)}(z)$. For this reason, the PP modification has to be calculated by the coupled wave equations:

DOI: 10.1021/acsphotonics.8b01467
ACS Photonics 2019, 6, 492−500

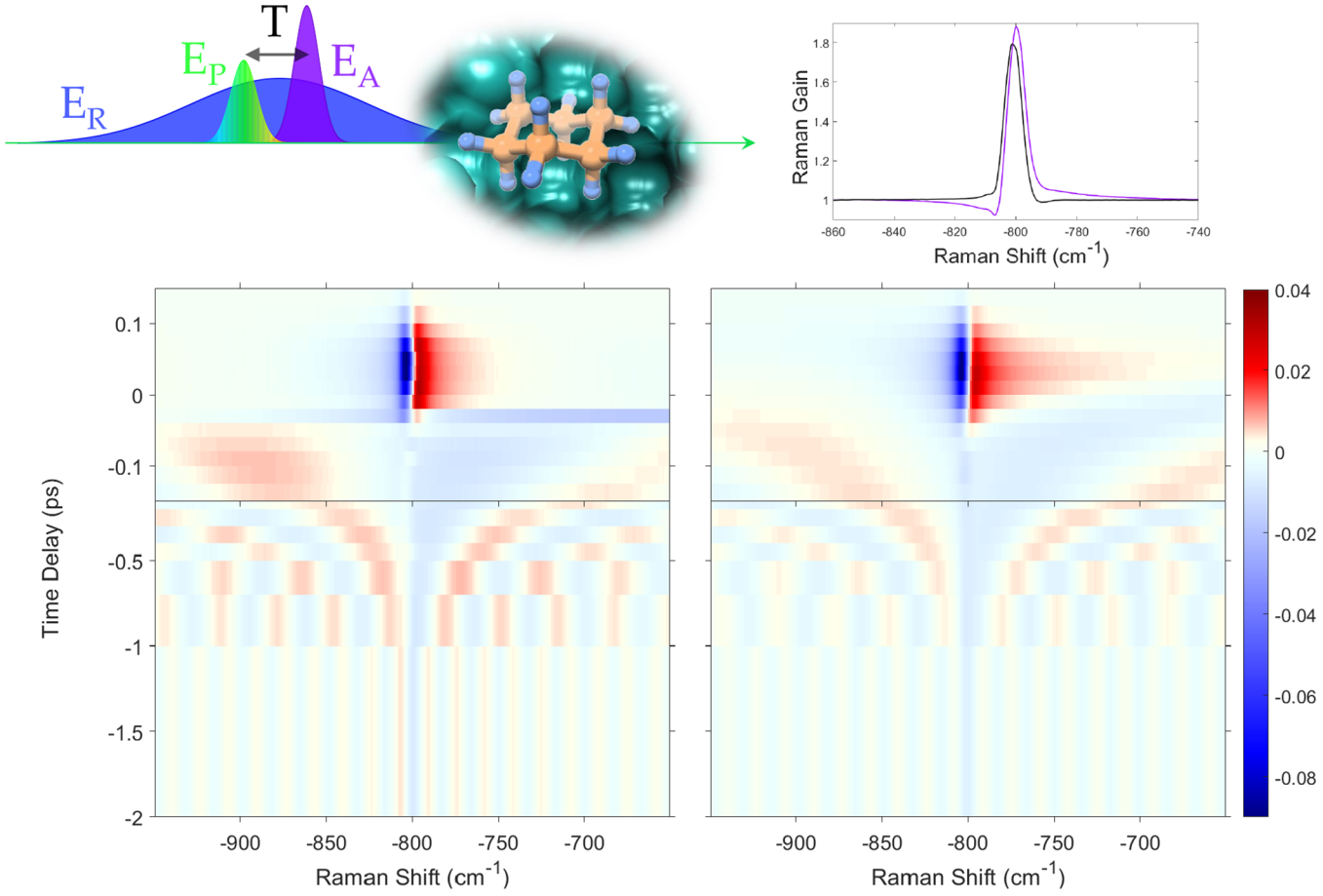

Figure 4. XPM artifacts in femtosecond broadband stimulated Raman as a function of the AP−PP relative delay: Experimental (left panel) and simulated (right panel) dependence of the nonresonant differential FSRS spectrum ΔRG on the relative delay between actinic and probe pulses for the 801 cm^{-1} Raman mode of liquid cyclohexane. The relative time delay between PP and RP is ΔT_{R-P} = 0.9 ps. A zoom-in on the time delay has been used for −150 fs < T < 120 fs, in order to emphasize the dispersive profile arising within the AP−PP time overlap regime. The inset shows a slice of the experimental Raman gain measured with and without the AP for T = 0 (purple and black lines, respectively).

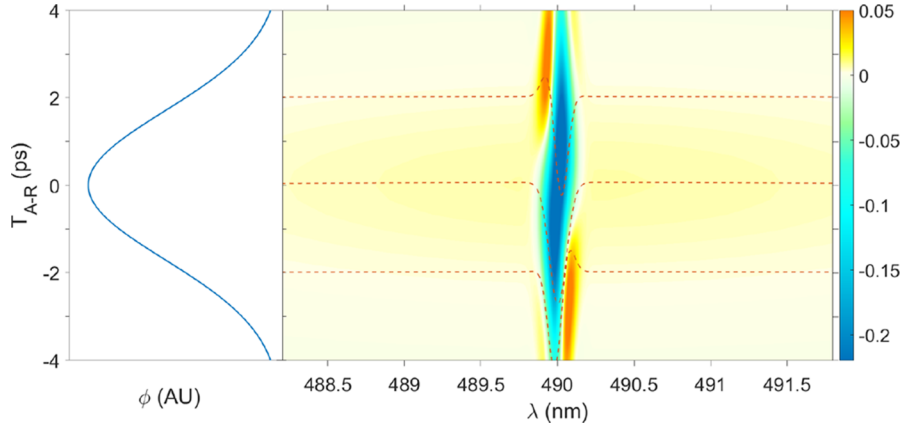

Figure 5. Spectral modification of the RP induced by XPM. The color map shows the simulated differential Raman pulse spectrum $\Delta I_R(\omega, T_{A-R})$ as a function of the temporal delay T_{A-R} between RP and AP; dashed lines indicate slices of $\Delta I_R(\omega, T_{A-R})$ at selected time delays. When T_{A-R} = 0, the RP spectrum undergoes a broadening and a decrease of the peak amplitude. For a nonvanishing T_{A-R}, $\Delta I_R(\omega)$ shows a dispersive profile, characterized by an odd symmetry for an AP preceding or following the RP maximum and indicating the induced frequency shift. The RP undergoes a red or a blue shift for positive or negative time delays, respectively. In the left panel the XPM-induced phase is reported as a function of T_{A-R}.

DOI: 10.1021/acsphotonics.8b01467
ACS Photonics 2019, 6, 492−500

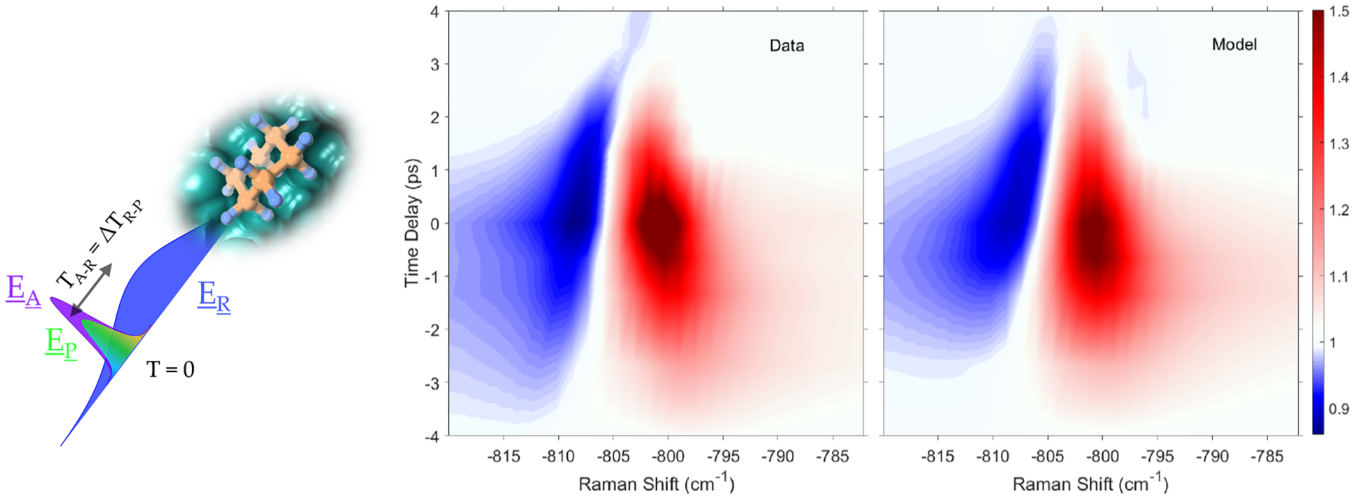

Figure 6. Femtosecond broadband stimulated Raman spectrum as a function of the femtosecond−picosecond pulses' relative delay. XPM artifacts are evaluated for an AP−PP pair overlapped and scanned along the RP temporal profile. Experimental and simulated spectral dependence is shown in liquid cyclohexane for the 801 cm^{-1} Raman mode.

$$
\begin{cases}
\dfrac{\partial^2 E_P}{\partial z^2} - \dfrac{1}{c^2}\dfrac{\partial^2 E_P}{\partial t^2} = \mu_0 \dfrac{\partial^2 P^{(3)}}{\partial t^2} \\
P^{(3)}(z,\omega) = |\mu_{ab}|^2 |\mu_{bc}|^2 \dfrac{1}{\tilde{\omega}_{bc} - \omega} \displaystyle\int_{-\infty}^{\infty} d\omega_1 \frac{\mathcal{E}_R^*(z,\omega_1)}{\omega_R + \omega_1 + \tilde{\omega}_{ab}} \\
\qquad \times \displaystyle\int_{-\infty}^{\infty} d\omega_3 \frac{\mathcal{E}_R(z,\omega_3)\mathcal{E}_P(z,\omega - \omega_P + \omega_1 - \omega_3)}{\omega - \omega_3 - \omega_R - \tilde{\omega}_{ac}} \\
\dfrac{\partial A_P}{\partial z} + \beta_1^{(P)}\dfrac{\partial A_P}{\partial t} + \dfrac{i}{2}\beta_2^{(P)}\dfrac{\partial^2 A_P}{\partial t^2} = i\gamma(|A_P|^2 + 2|A_A|^2)A_P \\
\dfrac{\partial A_R}{\partial z} + \beta_1^{(R)}\dfrac{\partial A_R}{\partial t} + \dfrac{i}{2}\beta_2^{(R)}\dfrac{\partial^2 A_R}{\partial t^2} = i\gamma(|A_R|^2 + 2|A_A|^2)A_R \\
\dfrac{\partial A_A}{\partial z} + \beta_1^{(A)}\dfrac{\partial A_A}{\partial t} + \dfrac{i}{2}\beta_2^{(A)}\dfrac{\partial^2 A_A}{\partial t^2} = i\gamma(|A_A|^2)A_A
\end{cases}
\tag{9}
$$

from which the femtosecond stimulated Raman gain (FSRG) can be calculated as

$$
\mathrm{FSRG}(\omega) = \frac{|E_P(\omega, L) - E_P(\omega, 0)|^2}{|E_P^0(\omega, 0)|^2} - 1 \tag{10}
$$

where $E_P(\omega, L)$ and $E_P(\omega, 0)$ represent the PP electromagnetic field at the entrance ($z = 0$) and at the output ($z = L$) of the sample.

In Figure 4 the experimental signal (left panels) is compared with the one modeled by means of eqs 9 and 10 (right panel), showing a good agreement and confirming that the differences ΔRG in the FSRS spectrum due to the presence of the AP should be ascribed to XPM artifacts between the AP and RP. The cyclohexane index of refraction used in the simulation has been taken from ref 48, while the integration step used is $dz/2$ = 12.5 μm.

XPM induces a spectral broadening of the RP, accompanied by a shift toward the red or the blue wavelengths, depending on the relative delay between AP and RP, T_{A-R}.[38] This is elucidated in Figure 5, where we report the simulated RP spectral modifications due to XPM, evaluated as the difference $\Delta I_R(\omega, T_{A-R})$ between the RP spectrum simulated in the presence and absence of the AP.

In the adopted experimental configuration, in order to enhance the RG and improve the spectral resolution,[39,40] the PP precedes the RP maximum, which is delayed by ΔT_{R-P} = 0.9 ps. Under these conditions, the AP−PP overlap corresponds to a delayed RP with respect to the AP, leading to an XPM-induced red shift of the RP. Therefore, the dispersive profile observed in Figure 4 for coincident AP and PP may be in principle ascribed to the RP frequency red shift. Notably, for a vanishing T_{A-R}, the RP undergoes a broadening, without any spectral shift (i.e., no modifications of the RP central frequency occur). Based on such considerations, a compelling hypothesis is that XPM artifacts can be avoided for $T_{A-R} = 0$, expecting no peak shifts in the overlap regime $T = 0$; accordingly, the dispersive profile, measured for an overlapping AP−PP pair, should also change symmetry for a PP temporally following the RP maximum.

To verify this hypothesis, we performed FSRS measurements at fixed $T = 0$ (i.e., for overlapped AP−PP), as a function of the time delay $\Delta T_{R-P} = T_{A-R}$ between the RP and the overlapped AP−PP pair, moving the RP temporal position. A sketched depiction of the experimental procedure is reported in the left panel of Figure 6. At odds with what is expected, the dispersive profile is maximum for $T \approx 0$ and does not change its symmetry upon scanning the RP temporal position across the AP−PP couple, as shown in the experimental FSRS spectrum reported in Figure 6 together with the one modeled by means of eqs 9 and 10. Notably, the experimental signal shows a good agreement with the model, indicating that the FSRS spectral modifications induced by XPM do not mimic the RP spectral shift. Hence it is not possible to predict XPM artifacts measuring the RP modifications and the full derivation of the FSRS signal should be extracted by means of eq 9. In fact, besides the spectral modification of the RP spectrum, XPM induces also a time-dependent phase $\phi(T)$ in the $E_R(t)$ electromagnetic field (see the left panel of Figure 5). While the central frequency of the RP undergoes a small absolute peak shift without sensibly affecting the FSRS spectra, the phase acquired by the RP is the effect responsible for the artifacts in the measured FSRS spectra. The presence of an additional phase factor, which modifies the portion of the RP temporally overlapped with the AP, can alter both the RP field−matter interactions appearing in the diagrams of Figure 2. Since the first interaction with the off-resonant RP field promotes the system to a virtual state, which "instantaneously" decays as it

DOI: 10.1021/acsphotonics.8b01467
ACS Photonics 2019, 6, 492−500

interacts with the PP, it involves only photons of the RP field temporally overlapped with the PP. For this reason, the first RP field−matter interaction is affected by XPM only during the AP−PP overlap regime, and it is responsible for the dispersive profiles measured around $T = 0$ reported in Figures 4 and 6. On the contrary, the third interaction with the RP occurs within the residual duration of the RP—after the stimulation of the vibrational coherence by the PP—and the dephasing time. For this reason, a larger portion of the RP modified by an AP following the PP is involved in the third field−matter interaction, which perturbs FSRS spectra and generates the oscillating contributions at $T < 0$.

CONCLUSIONS

In this paper, we have investigated the role of cross phase modulation in FSRS signals. The third-order nonlinear polarization generating SRS signals has been evaluated by a quantum treatment of matter through a perturbative expansion of the density matrix, while the pulse propagation inside the nonlinear medium has been evaluated using coupled wave equations. We have theoretically shown and experimentally demonstrated that, even in the off-resonance regime and without any photoinduced dynamics, time-dependent features arise in FSRS spectra due to XPM artifacts, which can hamper the detection and the interpretation of the system dynamics. In particular, we have identified two different regimes for XPM contributions: (i) for an AP following the PP, broad oscillating features arise around the Raman peaks; (ii) when the AP and PP are no longer well separated, dispersive features, centered around the peak positions, alter the positions and the line shapes of the Raman modes. The two effects can be explained by explicitly considering the modification of the phase of the Raman pulse during the two light−matter interactions involving the cross phase-modulated RP. The presented model can be applied to calculate the XPM artifacts also in the presence of a resonant photochemical pump, used in time-resolved inquiries for triggering a reaction of interest. Under such regimes, the FSRS spectra recorded during the time overlap between pump and probe contain both XPM artifacts and the spectral modifications induced by the system dynamics. Notably, since for negative time delays no photoinduced transient dynamics are present in the FSRS spectra, the oscillating features described and modeled in this paper can be fitted to extract the parameters relative to the XPM effects. Then these parameters can be used in the model to exactly calculate the XPM-induced modifications within the PP−AP overlap regime and remove them from the spectroscopic signal. Our work consequently enables disentangling and subtracting XPM artifacts from genuine dynamics in FSRS, in order to access the ultrafast processes occurring on temporal realms comprised within the AP−PP overlap regimes, which are particularly relevant in both the fields of photonics and solid state systems as well as the investigation of ultrafast dynamics in molecular compounds.

METHODS

Experimental Setup. A Ti:sapphire laser generates 3.6 mJ, 35 fs pulses at 800 nm and 1 kHz repetition rate. A portion of the laser fundamental drives a two-stage optical parametric amplifier (OPA) to generate a 650 nm, 60 fs actinic pump with 0.4 μJ energy on the sample. The Raman pulses are synthesized from a second two-stage OPA that produces tunable IR−visible pulses, followed by a spectral compression stage based on frequency doubling in a 25 mm beta barium borate crystal.[49] Cleaning of the RP spectral profile is performed by a double-pass 2f spectral filter, which enables at the same time reducing the pulse bandwidth and rectifying its temporal profile, increasing its time duration.[50,51] Raman pulses with 490 nm wavelength, 1 μJ energy, and 3.5 ps time duration are focused on the sample. The optical path consists of a 5 mm thick cyclohexane sample, contained in an optical glass cuvette (with constant transmission of more than 80% in the 400−800 nm spectral range). The AP and the RP pulses are collinear, while the PP is tilted by ∼2°. For simulating the signals reported here, we used an effective length $L = 1$ mm, taking into account the finite beam overlap region. The femtosecond probe is a white-light continuum (WLC), generated by focusing the laser fundamental into a sapphire crystal, and covers the 450−750 nm spectral range. The Raman features arise as positive gain on top of the transmitted WLC, which is frequency dispersed by a spectrometer onto a CCD device, able to perform single-shot acquisitions. A synchronized chopper at 500 Hz blocks alternating RP pulses in order to obtain the Raman gain using successive probe pulses, while a second chopper blocks the actinic pump at 250 Hz in order to obtain Raman gain spectra with and without actinic excitation. Notably, under the presented configuration, the stimulated Raman gain is calculated as the ratio of the PP with and without the RP in the presence of the AP, and hence eventual XPM effects on the PP do not affect the measured FSRS spectrum. All the pulses are linearly and parallel polarized. The temporal delays between the three pulses used in the FSRS experiment (indicated in Figure 2) can be tuned by means of two delay line stages (on the PP and AP beam paths).

ASSOCIATED CONTENT

Supporting Information

The Supporting Information is available free of charge on the ACS Publications website at DOI: 10.1021/acsphotonics.8b01467.

> Sample parameters; slices of Figure 1 for selected time delays; FSRS spectra at selected time delays; spectral and temporal dependence of differential FSRS spectra on linear and quadratic dispersion terms; stimulated Raman gain and differential FSRS spectral dependence on the RP and AP intensities; XPM artifacts' spectral dependence on the sample thickness (PDF)

AUTHOR INFORMATION

Corresponding Author

*E-mail: tullio.scopigno@phys.uniroma1.it.

ORCID

Giuseppe Fumero: 0000-0001-6836-8475
Carino Ferrante: 0000-0002-6391-0672
Shaul Mukamel: 0000-0002-6015-3135
Tullio Scopigno: 0000-0002-7437-4262

Notes

The authors declare no competing financial interest.

ACKNOWLEDGMENTS

S.M. acknowledges the support of the National Science Foundation (grant CHE-1361516).

DOI: 10.1021/acsphotonics.8b01467
ACS Photonics 2019, 6, 492−500

REFERENCES

(1) Baskin, J. S.; Zewail, A. H. Freezing Atoms in Motion: Principles of Femtochemistry and Demonstration by Laser Stroboscopy. *J. Chem. Educ.* **2001**, *78*, 737−751.

(2) Mizutani, Y. Direct Observation of Cooling of Heme Upon Photodissociation of Carbonmonoxy Myoglobin. *Science* **1997**, *278*, 443−446.

(3) Kruglik, S. G.; Lambry, J.-C.; Martin, J.-L.; Vos, M. H.; Negrerie, M. Sub-picosecond Raman spectrometer for time-resolved studies of structural dynamics in heme proteins. *J. Raman Spectrosc.* **2011**, *42*, 265−275.

(4) Versteeg, R. B.; Zhu, J.; Padmanabhan, P.; Boguschewski, C.; German, R.; Goedecke, M.; Becker, P.; van Loosdrecht, P. H. M. A tunable time-resolved spontaneous Raman spectroscopy setup for probing ultrafast collective excitation and quasiparticle dynamics in quantum materials. *Struct. Dyn.* **2018**, *5*, 044301.

(5) Yoshizawa, M.; Kubo, M.; Kurosawa, M. Ultrafast photo-isomerization in DCM dye observed by new femtosecond Raman spectroscopy. *J. Lumin.* **2000**, *87*, 739.

(6) Dietze, D. R.; Mathies, R. A. Femtosecond Stimulated Raman Spectroscopy. *ChemPhysChem* **2016**, *17*, 1224−1251.

(7) Kukura, P. Structural Observation of the Primary Isomerization in Vision with Femtosecond-Stimulated Raman. *Science* **2005**, *310*, 1006−1009.

(8) Laimgruber, S.; Schachenmayr, H.; Schmidt, B.; Zinth, W.; Gilch, P. A femtosecond stimulated raman spectrograph for the near ultraviolet. *Appl. Phys. B: Lasers Opt.* **2006**, *85*, 557−564.

(9) Pontecorvo, E.; Ferrante, C.; Elles, C. G.; Scopigno, T. Structural Rearrangement Accompanying the Ultrafast Electrocyclization Reaction of a Photochromic Molecular Switch. *J. Phys. Chem. B* **2014**, *118*, 6915−6921.

(10) Hall, C. R.; Conyard, J.; Heisler, I. A.; Jones, G.; Frost, J.; Browne, W. R.; Feringa, B. L.; Meech, S. R. Ultrafast Dynamics in Light-Driven Molecular Rotary Motors Probed by Femtosecond Stimulated Raman Spectroscopy. *J. Am. Chem. Soc.* **2017**, *139*, 7408−7414.

(11) Fang, C.; Frontiera, R. R.; Tran, R.; Mathies, R. A. Mapping GFP structure evolution during proton transfer with femtosecond Raman spectroscopy. *Nature* **2009**, *462*, 200−204.

(12) McCamant, D. W. Re-Evaluation of Rhodopsin's Relaxation Kinetics Determined from Femtosecond Stimulated Raman Lineshapes. *J. Phys. Chem. B* **2011**, *115*, 9299−9305.

(13) Kuramochi, H.; Takeuchi, S.; Tahara, T. Ultrafast Structural Evolution of Photoactive Yellow Protein Chromophore Revealed by Ultraviolet Resonance Femtosecond Stimulated Raman Spectroscopy. *J. Phys. Chem. Lett.* **2012**, *3*, 2025−2029.

(14) Ferrante, C.; Pontecorvo, E.; Cerullo, G.; Vos, M. H.; Scopigno, T. Direct observation of subpicosecond vibrational dynamics in photoexcited myoglobin. *Nat. Chem.* **2016**, *8*, 1137−1143.

(15) Takaya, T.; Anan, M.; Iwata, K. Vibrational relaxation dynamics of β-carotene and its derivatives with substituents on terminal rings in electronically excited states as studied by femtosecond time-resolved stimulated Raman spectroscopy in the near-IR region. *Phys. Chem. Chem. Phys.* **2018**, *20*, 3320−3327.

(16) Zhou, J.; Yu, W.; Bragg, A. E. Structural Relaxation of Photoexcited Quaterthiophenes Probed with Vibrational Specificity. *J. Phys. Chem. Lett.* **2015**, *6*, 3496−3502.

(17) Batignani, G.; Pontecorvo, E.; Ferrante, C.; Aschi, M.; Elles, C. G.; Scopigno, T. Visualizing Excited-State Dynamics of a Diaryl Thiophene: Femtosecond Stimulated Raman Scattering as a Probe of Conjugated Molecules. *J. Phys. Chem. Lett.* **2016**, *7*, 2981−2988.

(18) Barclay, M. S.; Quincy, T. J.; Williams-Young, D. B.; Caricato, M.; Elles, C. G. Accurate Assignments of Excited-State Resonance Raman Spectra: A Benchmark Study Combining Experiment and Theory. *J. Phys. Chem. A* **2017**, *121*, 7937−7946.

(19) Roy, K.; Kayal, S.; Kumar, V. R.; Beeby, A.; Ariese, F.; Umapathy, S. Understanding Ultrafast Dynamics of Conformation Specific Photo-Excitation: A Femtosecond Transient Absorption and Ultrafast Raman Loss Study. *J. Phys. Chem. A* **2017**, *121*, 6538−6546.

(20) Quick, M.; Dobryakov, A. L.; Kovalenko, S. A.; Ernsting, N. P. Resonance Femtosecond-Stimulated Raman Spectroscopy without Actinic Excitation Showing Low-Frequency Vibrational Activity in the S 2 State of All-Trans β-Carotene. *J. Phys. Chem. Lett.* **2015**, *6*, 1216−1220.

(21) Hontani, Y.; Kloz, M.; Polívka, T.; Shukla, M. K.; Sobotka, R.; Kennis, J. T. M. Molecular Origin of Photoprotection in Cyanobacteria Probed by Watermarked Femtosecond Stimulated Raman Spectroscopy. *J. Phys. Chem. Lett.* **2018**, *9*, 1788−1792.

(22) Piontkowski, Z.; McCamant, D. W. Excited-State Planarization in Donor-Bridge Dye Sensitizers: Phenylene versus Thiophene Bridges. *J. Am. Chem. Soc.* **2018**, *140*, 11046−11057.

(23) Hannah, D. C.; Brown, K. E.; Young, R. M.; Wasielewski, M. R.; Schatz, G. C.; Co, D. T.; Schaller, R. D. Direct Measurement of Lattice Dynamics and Optical Phonon Excitation in Semiconductor Nanocrystals Using Femtosecond Stimulated Raman Spectroscopy. *Phys. Rev. Lett.* **2013**, *111*, 107401.

(24) Provencher, F.; Bérubé, N.; Parker, A. W.; Greetham, G. M.; Towrie, M.; Hellmann, C.; Côté, M.; Stingelin, N.; Silva, C.; Hayes, S. C. Direct observation of ultrafast long-range charge separation at polymer−fullerene heterojunctions. *Nat. Commun.* **2014**, *5*, DOI: 10.1038/ncomms5288.

(25) Cinchetti, M. Between two spins. *Nat. Photonics* **2015**, *9*, 489−490.

(26) Batignani, G.; Bossini, D.; Palo, N. D.; Ferrante, C.; Pontecorvo, E.; Cerullo, G.; Kimel, A.; Scopigno, T. Probing ultrafast photo-induced dynamics of the exchange energy in a Heisenberg antiferromagnet. *Nat. Photonics* **2015**, *9*, 506−510.

(27) Kukura, P.; McCamant, D. W.; Mathies, R. A. Femtosecond Stimulated Raman Spectroscopy. *Annu. Rev. Phys. Chem.* **2007**, *58*, 461−488.

(28) Mukamel, S.; Biggs, J. D. Communication: Comment on the effective temporal and spectral resolution of impulsive stimulated Raman signals. *J. Chem. Phys.* **2011**, *134*, 161101.

(29) Fumero, G.; Batignani, G.; Dorfman, K. E.; Mukamel, S.; Scopigno, T. On the Resolution Limit of Femtosecond Stimulated Raman Spectroscopy: Modelling Fifth-Order Signals with Overlapping Pulses. *ChemPhysChem* **2015**, *16*, 3438−3443.

(30) Kovalenko, S. A.; Dobryakov, A. L.; Ruthmann, J.; Ernsting, N. P. Femtosecond spectroscopy of condensed phases with chirped supercontinuum probing. *Phys. Rev. A: At., Mol., Opt. Phys.* **1999**, *59*, 2369−2384.

(31) Liebel, M.; Schnedermann, C.; Wende, T.; Kukura, P. Principles and Applications of Broadband Impulsive Vibrational Spectroscopy. *J. Phys. Chem. A* **2015**, *119*, 9506−9517.

(32) Musser, A. J.; Liebel, M.; Schnedermann, C.; Wende, T.; Kehoe, T. B.; Rao, A.; Kukura, P. Evidence for conical intersection dynamics mediating ultrafast singlet exciton fission. *Nat. Phys.* **2015**, *11*, 352−357.

(33) Monacelli, L.; Batignani, G.; Fumero, G.; Ferrante, C.; Mukamel, S.; Scopigno, T. Manipulating Impulsive Stimulated Raman Spectroscopy with a Chirped Probe Pulse. *J. Phys. Chem. Lett.* **2017**, *8*, 966−974.

(34) Batignani, G.; et al. Probing femtosecond lattice displacement upon photo-carrier generation in lead halide perovskite. *Nat. Comm.* **2018**, *9*, 1971.

(35) Lim, S.; et al. Spectral modulation of stimulated Raman scattering signal: Beyond weak Raman pump limit. *J. Raman Spectrosc.* **2018**, *49* (4), 607−620.

(36) Agrawal, G. *Nonlinear Fiber Optics*; Academic Press, 2013.

(37) Agrawal, G. P.; Baldeck, P. L.; Alfano, R. R. Temporal and spectral effects of cross-phase modulation on copropagating ultrashort pulses in optical fibers. *Phys. Rev. A: At., Mol., Opt. Phys.* **1989**, *40*, 5063−5072.

(38) Baldeck, P. L.; Alfano, R. R.; Agrawal, G. P. Induced frequency shift of copropagating ultrafast optical pulses. *Appl. Phys. Lett.* **1988**, *52*, 1939−1941.

(39) Yoon, S.; McCamant, D. W.; Kukura, P.; Mathies, R. A.; Zhang, D.; Lee, S.-Y. Dependence of line shapes in femtosecond broadband

DOI: 10.1021/acsphotonics.8b01467
ACS Photonics 2019, 6, 492−500

stimulated Raman spectroscopy on pump-probe time delay. *J. Chem. Phys.* **2005**, *122*, 024505.
(40) Ferrante, C.; Batignani, G.; Fumero, G.; Pontecorvo, E.; Virga, A.; Montemiglio, L. C.; Cerullo, G.; Vos, M. H.; Scopigno, T. Resonant broadband stimulated Raman scattering in myoglobin. *J. Raman Spectrosc.* **2018**, *49*, 913−920.
(41) Lee, S.-Y.; Zhang, D.; McCamant, D. W.; Kukura, P.; Mathies, R. A. Theory of femtosecond stimulated Raman spectroscopy. *J. Chem. Phys.* **2004**, *121*, 3632−3642.
(42) Batignani, G.; Fumero, G.; Mukamel, S.; Scopigno, T. Energy flow between spectral components in 2D broadband stimulated Raman spectroscopy. *Phys. Chem. Chem. Phys.* **2015**, *17*, 10454−10461.
(43) Mukamel, S. *Principles of Nonlinear Spectroscopy*; Oxford University Press, 1995.
(44) Dorfman, K. E.; Fingerhut, B. P.; Mukamel, S. Time-resolved broadband Raman spectroscopies: A unified six-wave-mixing representation. *J. Chem. Phys.* **2013**, *139*, 124113.
(45) Batignani, G.; Pontecorvo, E.; Giovannetti, G.; Ferrante, C.; Fumero, G.; Scopigno, T. Electronic resonances in broadband stimulated Raman spectroscopy. *Sci. Rep.* **2016**, *6*, DOI: 10.1038/srep18445.
(46) Gardecki, J. A.; Constantine, S.; Zhou, Y.; Ziegler, L. D. Optical heterodyne detected spectrograms of ultrafast nonresonant electronic responses. *J. Opt. Soc. Am. B* **2000**, *17*, 652−662.
(47) Boyd, R. W. *Nonlinear Optics*, third ed.; Academic Press, 2008.
(48) Rheims, J.; Köser, J.; Wriedt, T. Refractive-index measurements in the near-IR using an Abbe refractometer. *Meas. Sci. Technol.* **1997**, *8*, 601−605.
(49) Pontecorvo, E.; Kapetanaki, S.; Badioli, M.; Brida, D.; Marangoni, M.; Cerullo, G.; Scopigno, T. Femtosecond stimulated Raman spectrometer in the 320−520nm range. *Opt. Express* **2011**, *19*, 1107−1112.
(50) Pontecorvo, E.; Ferrante, C.; Elles, C. G.; Scopigno, T. Spectrally tailored narrowband pulses for femtosecond stimulated Raman spectroscopy in the range 330−750 nm. *Opt. Express* **2013**, *21*, 6866−6872.
(51) Hoffman, D. P.; Valley, D.; Ellis, S. R.; Creelman, M.; Mathies, R. A. Optimally shaped narrowband picosecond pulses for femtosecond stimulated Raman spectroscopy. *Opt. Express* **2013**, *21*, 21685−21692.

DOI: 10.1021/acsphotonics.8b01467
ACS Photonics 2019, 6, 492−500